Mining of Mineral Deposits
Volume 19 (2025), Issue 3, 87-97

MMD JOURNAL / MINING.IN.UA

https://doi.org/10.33271/mining19.03.087

Modeling cave propagation in deep block caving by incorporating the fracture zone inferred from seismic tomography

Sari Melati [1,2*], Ridho K. Wattimena [1], David P. Sahara [1], Ganda M. Simangunsong [1], Adi Wibowo [3], Wahyu Hidayat [4], Erwin Riyanto [5]

[1] *Institut Teknologi Bandung, Bandung, Indonesia*
[2] *Universitas Lambung Mangkurat, Banjarbaru, Indonesia*
[3] *Universitas Diponegoro, Semarang, Indonesia*
[4] *Universitas Pembangunan Nasional Veteran Yogyakarta, Yogyakarta, Indonesia*
[5] *PT Freeport Indonesia, Mimika, Indonesia*

**Corresponding author: e-mail sari@ulm.a.cid*

Abstract

Purpose. This study aims to enhance the monitoring of cave propagation in block caving developments by integrating microseismic tomography for numerical modeling of rock mass evolution due to mining and displacement distribution.

Methods. This study used the low-velocity zone identified by four-dimensional tomography as a fracturing or loosening zone near the cave boundary. The elastic properties of the fractured zone were adjusted to analyze their impacts on stress and displacement distribution. The displacement models for each scenario were validated using observed time-domain reflectometry (TDR).

Findings. The reduction in rock mass deformation modulus, inferred from decreased seismic wave velocity, produced a displacement distribution consistent with Time Domain Reflectometer (TDR) measurements. The quantified reduction in rock mass deformation modulus within the zone of loosening or low velocity (4.5 km/s) was approximately 0.5 times the intact rock modulus. The northwestern cave boundary, predicted to expand, was accurately modelled as the rock mass zone with the highest displacement (19 cm), coinciding with the induced stress concentration and high stress-strain localization in that area.

Originality. Conventional stress – strain – displacement numerical modeling typically assumes constant rock mass properties. However, during the caving process, extensive fracture growth and extension transform the rock mass from intact to highly jointed, significantly altering its mechanical behavior. This study proposes a new integrated method utilizing rock velocity models from microseismic monitoring to modify the rock mass deformation modulus in numerical modeling, during the fracturing stage under high cave-mining-induced stress conditions.

Practical implications. This study successfully optimized the use of microseismic monitoring data to update rock mass conditions within the fracturing zone. This approach allows the elastic properties used in numerical modeling to be time-lapse representative and to incorporate the effects of fracturing progression.

Keywords: *cave propagation, fracture zones, numerical modeling, seismic tomography, underground mining*

1. Introduction

Block caving is recognized as the most efficient technique for massive underground mining operations [1]. This method has gained popularity alongside advancements in mining technology, rock engineering, quality control, and safety measures [2]-[6]. The sustainability of mine production and safety increasingly relies on enhanced monitoring techniques. Monitoring in cave mines presents unique challenges compared to that in other underground mining methods because of the extensive excavation dimensions and the prolonged operational lifespan of mines. Notably, caves are often constructed beneath existing open pits in contemporary practices, with subsequent excavations around the initial cave. This process complicates the induced stress conditions within the rock mass owing to the interactions among the caves [7]. Therefore, cave mines necessitate monitoring methods that can survey extensive areas deep within the rock masses, far from any exposed rock in tunnels.

Microseismic monitoring is a critical tool in cave mines, used to identify zones at risk of rock bursts, characterize seismic activity, and map stress redistribution, among other objectives [8], [9]. Seismic tomography, as an advanced data-processing technique, enhances the informativeness and reliability of seismic data for monitoring velocity variations [10]. These velocity variations are crucial properties that determine the geophysical condition of the rock surrounding the cave, as demonstrated in the back-analysis of microseismic events and stress analyses.

The primary focus in cave mining monitoring is cave propagation, which serves as a key indicator of production

Received: 18 January 2025. Accepted: 8 September 2025. Available online: 30 September 2025

Mining of Mineral Deposits. ISSN 2415-3443 (Online) | ISSN 2415-3435 (Print)

effectiveness. Mercier et al. (2015) developed a velocity model from passive seismic monitoring to trace the temporal evolution of cave geometry; however, their findings have not been validated against actual caving front data [11]. In a recent study, Hidayat et al. (2024) investigated cave propagation and stress distribution as indicated by clusters of seismic events [12]. By modeling the rock velocity tomogram based on bi-weekly observational data, they observed a decrease and contrast in the velocities of primary (V_p) and secondary (V_s) waves within the prospective caving zone. These findings confirm that seismic velocity measurements are critical in identifying areas of cave propagation.

A key challenge lies in optimizing the use of tomographic images to enhance the geotechnical understanding of underground mining, particularly concerning rock mass properties. Previous research, encompassing both lab-scale samples and field measurements, has established that rock velocity correlates with deformability [13]-[16]. Fracture frequency is densified by the presence of joints, which in turn reduces rock mass deformability [17]-[19]. A specific relationship between rock mass deformability and the ratio of rock mass velocity to that of intact rock was proposed by Coon and Merit (1970) as interpreted by Deere and Deere (1989) [20]. According to caving mechanics theory, the rock mass zone between the cave boundary and the seismogenic zone undergoes extensive fracturing, becoming more jointed than its initial state. This fracture zone at the cave boundary is referred to as the loosening zone or yielded zone [21]. In an elastic model, a jointed rock mass exhibits reduced strength and stiffness compared to a competent rock mass [22], [23]. Given that a low velocity indicates a weakened rock mass and that the caving mechanism involves a loosening zone at the cave boundaries, it is crucial to modify rock mass properties, especially deformability, using velocity data from tomography.

Numerical modeling has been extensively utilized in block caving studies to analyze influencing parameters on rock mass cavability [24], determine the caving hydraulic radius of rock mass [25], develop models of gravity flow [26], and investigate surface responses [27]-[29]. However, literature on numerical modeling involving rock damage due to cave induction is still limited.

In this study, rock velocity distribution was interpreted as an indicator of rock mass quality. Utilizing the velocity model and cave geometry from [12], this research analyzed displacement and cave propagation. The caving mechanism ensured that the low-velocity zone around cave boundaries corresponded to the loosening zone. Simulations of the fracture zone involved modifying the elastic properties of the rock mass to reflect conditions induced by block caving. The deformability of this fracture zone was assessed using the rock mass velocity model derived from tomographic data. A synthetic rock mass model was developed, accounting for depth variations, heterogeneous lithologies, and the typical cave geometry. This study also examined the impact of the fracture zone on displacement, proposing that the loosening and synthetic fracture zones can be effectively modeled using modified elastic properties; this, in turn, facilitates microseismic monitoring as a viable method for displacement modeling to predict cave propagation.

2. Methods

2.1. Engineering geology and mining situation in Deep Mill Level Zone

Numerical modeling in this study was derived from seismic tomography data specific to the block caving mining in the Deep Mill Level Zone (DMLZ). Figure 1 shows the block-caving mining method. In this approach, access tunnels and an extraction level are developed beneath the ore body.

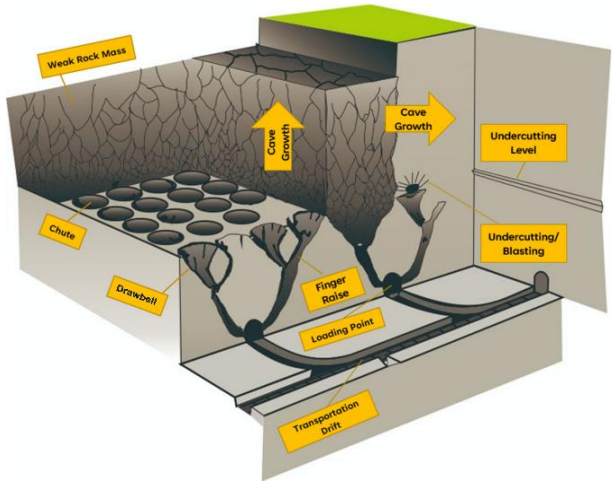

Figure 1. Layout of the block caving mining method

Above extraction level, an undercut level is designed to facilitate ore body breakage via drilling and blasting. Blasting and ore withdrawal at the undercut level are conducted in stages to cause the ore body to collapse due to gravity, aligning with the controlled and continuous collapse objectives of rock engineering in this mining method. The ore, once broken, is drawn and transported to the extraction level. The drawing activity at the undercut level results in the formation of a cavity above, which in turn triggers caving-induced stress. Once a specific hydraulic radius (the ratio of height to area of the cave) is achieved, the cave propagates continuously, allowing the broken ore to move by gravity, which enhances productivity in terms of production rate and cost.

The DMLZ is the deepest mine within the block caving complex of PT Freeport Indonesia, situated more than 1700 m below the surface. This mine targets the extraction of copper-gold and skarn deposits within the diorite intrusion of the East Erstberg Skarn System (EESS). The EESS represents a vertically continuous porphyry and skarn-type mineralized zone that develops at the contact zone between Erstberg diorite (Te) rocks and carbonate and siliciclastic wall rocks. This contact occurs along the northern edge of the Erstberg intrusion complex. The resulting alteration and rock units, consisting of skarn, hornfels, and dolomitic formations, arise from the interaction between the igneous rock and sedimentary limestone.

Figure 2 shows the rock units and geological structure of the DMLZ mine area. Geological map of the Deep Mill Level Zone (DMLZ) at 2600 meters above sea level (masl), showing the location of the DMLZ mine (modified from [12]). The DMLZ cave targets copper ore in the skarn and diorite deposits. The geological layers are primarily oriented northwest-southeast (NW-SE), influenced by the dominant structural forms of folds and faults in the area.

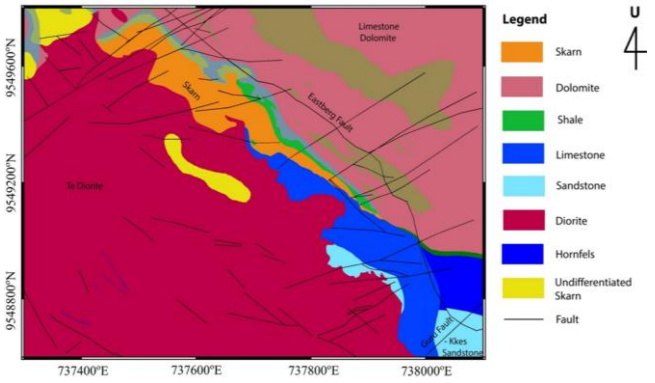

Figure 2. Geological map of the Deep Mill Level Zone (DMLZ)

The syncline structure and an up-fault both follow this NW-SE direction. Additionally, a paired shear fault occurs in the NW-SE and northeast-southwest (NE-SW) directions. The rock formations are angled at slopes ranging from moderate to steep, between 40 and 75°.

2.2. Model description

The cave model, representing the current state of the block cave mine, was developed based on findings by Hidayat et al. (2024) [12]. This block cave mine is situated at a depth of 1700 m and uses velocity tomography for monitoring purposes. The rock mass surrounding the cave comprises three heterogeneous materials with distinct properties: limestone, skarn, and diorite. These variations are due to the intrusion of diorite into sedimentary rock, which hosts copper-gold and skarn deposits.

The velocity model was constructed using seismic monitoring data through tomographic methods. Variations in velocity anomalies around the cave were periodically monitored, analyzing the evolution of P-wave (V_p), S-wave (V_s), and the V_p/V_s ratio. Figure 3 shows initial velocity model of the rock mass in the DMLZ, illustrating the cave model on heterogeneous rock masses (skarn, limestone, and diorite). The diorite, skarn, and limestone are depicted in red, dark blue, and light blue zones, respectively. The initial velocity model of the main lithologies limestone, skarn, and diorite in the DMLZ, with respective P-wave velocities of 6.23, 5.59, and 4.91 km/s.

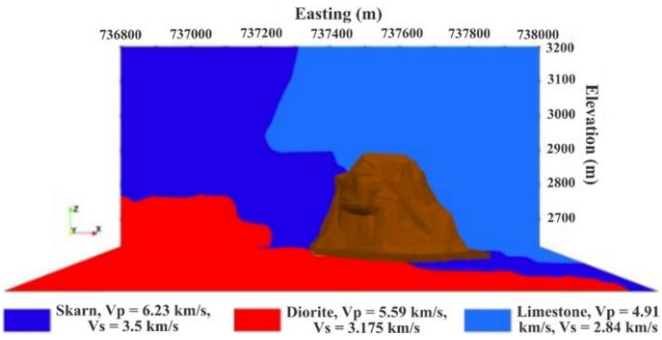

Figure 3. Initial velocity model of the rock mass in the DMLZ

The processing of seismic monitoring data through tomography provides an updated velocity model. As shown in the horizontal section at an elevation of 2700 masl (Fig. 4), this model indicates the stress distribution and caving mechanisms induced by caving. The velocity distribution model reveals a low-velocity zone in the northwest of the cave, attributed to pressure release and significant rock fracturing, which corresponds with a cave propagation of approximately 60 m, as inferred from tomography. Updated velocity model considering caving, derived from tomography by Hidayat et al. (2024) [12]. The velocity distribution contrasts with the initial model, particularly in the skarn lithology (predominantly dark blue) and diorite (predominantly cyan), where numerous seismic events occur. On the northwest side of the cave, specifically within the skarn lithology, a low-velocity zone (red zone) is modeled as a fractured rock mass.

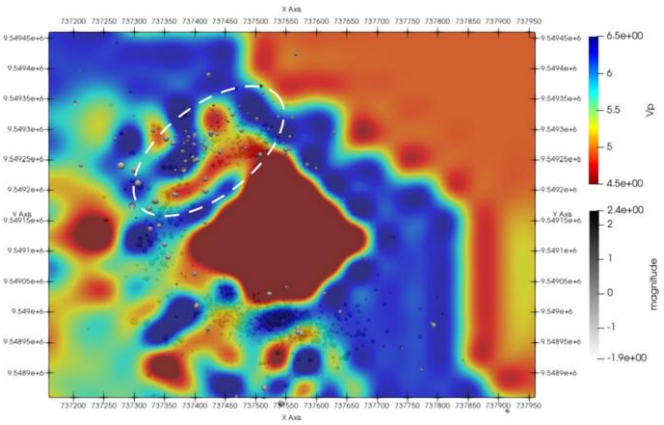

Figure 4. Updated velocity model considering caving, derived from tomography by Hidayat et al. (2024) [12]

Figure 5 shows a simplified interpretation of this velocity model. This schematic interprets the velocity model shown in Figure 4. The low-velocity zone to the northwest of the cave is interpreted as a fracturing skarn lithology or a loosening. According to this model, and considering that low velocity in hard rock suggests fracturing, a zone of weak rock mass has formed on the northwest side of the cave, induced by caving-related stress. This is indicated by the emergence and expansion of a low-velocity area in the northwest, observed six weeks prior to caving.

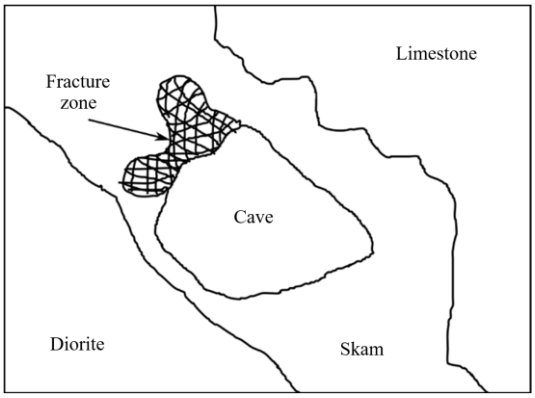

Figure 5. Simplified interpretation of the updated rock velocity model induced by caving mechanics

Based on the conceptual model of caving by Duplancic (1999) [22], the rock mass near the cave boundary, or the cave back, experiences continuous damage ([30] after [22]. Stress redistribution results in a seismogenic zone located at a specific distance from the cave boundary, where the damage rate diminishes. The boundaries between the damage zone and the seismogenic zone, as indicated in Figure 4, are delineated by transitions from a low-velocity (red) zone to a high-velocity (blue) zone.

In the rock mass on the northwest side of the cave, the red zone is encircled by the blue zone. The transition area, marked with a white dashed line, was seismically active, with events registering local magnitudes between -1.6 and 2. Therefore, we model a fracture zone near the boundary of the cave on the northwest side, as shown in Figure 5, identified by the low-velocity zone (red zone) in Figure 4.

The boundary of contrasting velocity around the low-velocity area is interpreted as a weakened rock mass resulting from high induced stress. Consequently, failure occurs at this boundary, subsequently defining the new shape of the cave. In this study, the sequence of rock mass fracturing phenomena was analyzed using numerical displacement modeling to account for the weakening of the rock mass.

The representative model for this block cave mine was developed using the finite-element method to analyze displacement and stress distribution. The low-velocity anomalies detected by four-dimensional (4D) time-lapse tomography in the northwest area were critical for defining the loosening zone as a result of rock mass evolution due to cave excavation, as shown in Figure 5. The numerical modeling conducted in this study incorporates the fracture zone in the calculations of stress and strain.

2.3. Model setting

The numerical model was developed to estimate the impact of rock mass variation on displacement around the cave. The modeling approach uses finite elements with RocScience3D (RS3) software, involving initial and boundary conditions, in situ stress, stiffness, strength, and mesh.

The initial condition is defined as a body force, representing the stress due to the unit weight of the rock mass itself, which determines the overburden pressure. The boundary condition is set as surface auto-restrain, ensuring the equilibrium of forces at the bottom and lateral external boundaries of the model. The surface boundary experiences in situ stress as an even load across the model surface, equating to gravity stress at a specified depth (Fig. 6).

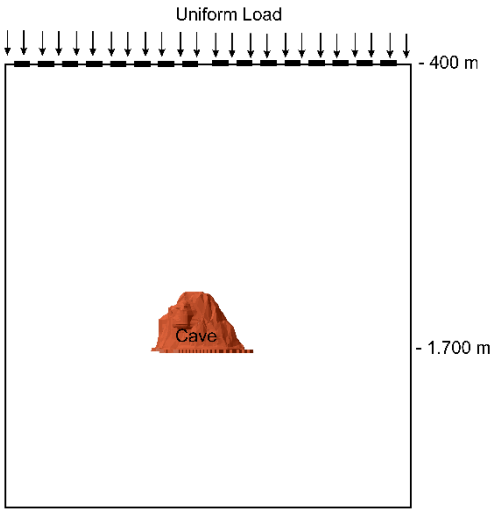

Figure 6. Two-dimensional illustration of the initial and boundary conditions of the numerical model

The cave, excavated at a depth of 1700 m, is modeled with displacement constrained to the lateral and lower boundaries owing to the infinite assumptions of the model. At the surface boundary (top side of the three-dimensional model), the model endures a uniform load equal to the vertical stress at a depth of 400 m below the surface. Stiffness behavior is modeled as isotropic linear, where stress and strain changes have a linear relationship, defined by Young's modulus and Poisson's ratio. These linear elastic properties are consistent in all directions, both laterally and vertically. The failure criterion used is the Mohr-Coulomb model, and the material type is elastic. In this model, the strength of a material is defined by its cohesion, friction angle, and tensile strength.

Three materials are modeled to represent three lithological zones oriented to the northwest with an almost vertical slope (Fig. 7). Three-dimensional model of the geometry of rock mass and cave, indicated by green space in the block. The cave is set as an excavation, with the blue, green, and red zones representing limestone, skarn, and diorite, respectively. These zones are set as geology and are bounded by vertical planes striking northwest (planes A and B). The cave consists of skarn lithology and is the primary mining target. The modeled cave features an undercut level measuring 364 × 282 m, with a height of approximately 300 m, narrowing towards the top to an average width of 200 m. The rock mass within the external boundary is modeled as a radius three times the dimensions of the cave, incorporating both the excavation and surrounding geology (diorite, skarn, and limestone). Excavation refers to the cave from the top to the footprint on the undercut level floor, while geology encompasses the rock mass around the cave, defined by its physical and mechanical properties within lithological boundaries.

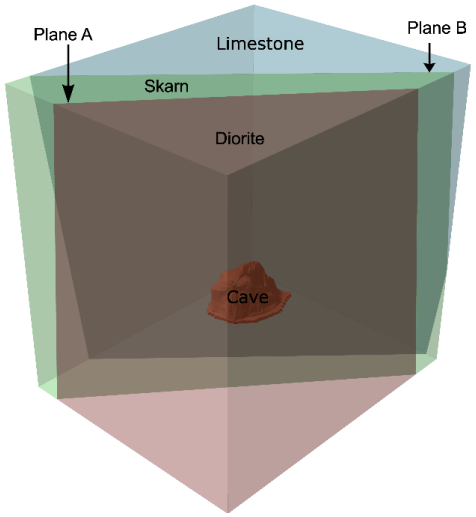

Figure 7. Three-dimensional model of the geometry of rock mass and cave

A mesh, the finest structure within a model, facilitates incremental computations by the numerical model. A four-node graded mesh gradually optimizes the computational process, building an irregular tetrahedral mesh with denser network points at the boundaries of cave geometry and lithological boundaries and tapering towards the outer limits of the model.

The material properties used in the rock mass model are listed in Table 1. These properties, estimated for the three lithologies, have been validated by references from previously published studies [31]-[33]. The properties include specific parameter inputs for initial conditions, stiffness, and strength for each lithology.

Table 1. Rock mass properties for modeling stress distribution and displacement

Main lithology	Unit weight, MN/m^3	Young's modulus, GPa	Poisson's ratio	Cohesion, MPa	Friction angle, degree	Tensile strength, MPa	Porosity, %
Diorite	0.025	48	0.21	19	54	9	0.6
Skarn	0.030	61	0.23	23	16	18	2.1
Limestone	0.029	58	0.23	21	35	9	0.7
Fracture zone	0.030	30.5	0.23	23	16	18	2.1
Plane A	0.0275	54.5	0.22	21	35	13.5	1.35
Plane B	0.0295	59.5	0.23	22	25.5	13.5	1.40

The properties assigned to the model are experimental values used to test the model. The primary objective of this modeling is to identify trends and directions in stress and displacement distribution resulting from the applied treatments in the model. For more precise analyses, such as assessing the magnitude of stress and displacement, the properties should be calibrated with actual site conditions. Intact rock properties were determined through laboratory measurements of samples drilled from the site location, including tests for uniaxial compressive strength, triaxial strength, tensile strength, and physical properties. To calibrate the laboratory results to represent the rock mass condition, the joint parameter on site is considered to adjust the mechanical properties.

The stiffness, represented by Young's Modulus, is 48, 61, and 58 MPa for diorite, skarn, and limestone, respectively. The strength is expressed by the uniaxial compressive strength (UCS), with values of 160, 135, and 95 MPa for diorite, skarn, and limestone, respectively. In RS3, the material strength according to the Mohr-Coulomb criterion is defined by cohesion, friction angle, and tensile strength. This model also considers the interface properties between each pair of lithologies. The boundaries between limestone and skarn, and between skarn and diorite, were modeled as planes with an approximate direction of N 40° E/90°, with assigned properties predicted from the average of the two contacted lithologies. Planes A and B, as listed in Table 1, limit the lithology corresponding to diorite-skarn and skarn-limestone, respectively.

Determining the mechanical properties of the fracture zone is a critical step in the modeling method proposed in this study. According to the velocity model, the northwest of the cave features a low-velocity zone with a velocity reduction of approximately 1.73 km/s compared to the competent rock velocity from skarn (6.23 km/s), resulting in a velocity index of approximately 0.72. Based on Coon and Merit (1970), a rock mass with a velocity index of 0.6-0.8 and a rock-quality designation (RQD) of 75-90% is estimated to have a modulus ratio ($E_{rock\ mass}$ / $E_{rock\ lab}$) ranging from 0.5-0.8 [20]. Further, according to empirical data analyzed by Zhang (2017) [21], with an RQD of 75-90%, the deformation modulus of the rock mass is approximately 0.3-0.5 of that of the intact rock. In this study, the deformation modulus in the fracture zone, including the low velocity or loosening zone in the northwest of the cave and the synthetic fracture zone in the southeast of the cave, is set at approximately 0.5 of the skarn deformation modulus, which is 30.5 MPa. Modifying the deformation modulus in the fracture zone aims to produce a displacement distribution model that more accurately reflects the conditions at the site.

2.4. Modeling scenario

In the block caving mining method, fracturing of competent rock mass is a natural and essential process for cave development; however, it must be controlled to align with the expected direction from the mining design. To examine various modeling methods for rock mass fracturing engineering around the cave, we conducted three distinct modeling scenarios in this study. The initial velocity model serves as a reference to construct a three-dimensional model for scenario I, featuring only a cave in the skarn lithology flanked by diorite and limestone. Scenario II introduces a fracture zone or loosening zone on the northwest side of the cave, as inferred from the velocity model's interpretation. The deformation modulus properties assigned to the loosening zone reflect empirical relationships between wave velocity and rock mass quality. The displacement results from scenarios I and II are compared with measured changes in the cave through time-domain reflectometry (TDR) data. Scenario III adds a synthetic fracture zone on the southeast side of the cave, opposite the loosening zone, to simulate displacement due to the interaction of the two fracture zones with the cave.

Differences in model reference and geometric treatment between the three models are shown in Figure 8. Simplified reference models of scenarios I, II, and III along the northwest-southeast cross-section.

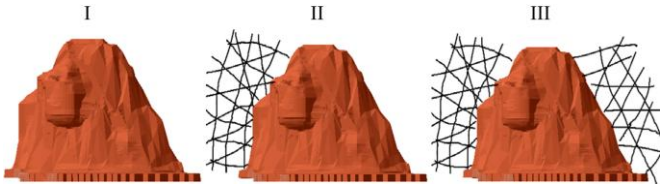

Figure 8. Simplified reference models of scenarios I, II, and III

Scenario I models displacement due to cave excavation. Scenario II models displacement due to cave excavation and the loosening zone northeast of the cave. Scenario III models displacement due to cave excavation and the interaction between the loosening zone in the northwest of the cave and the synthetic fracture zone in the southeast, indicated by crossed lines on the northwest and southeast sides of the cave. The model settings for the three scenarios are as follows:

I – hard rock mass properties represented by the competent rock mass's properties;

II – the loosening zone modeled as a volume of rock mass on the southwest side of the cave that experienced a reduction in deformation modulus (Young's Modulus) based on empirical data;

III – a synthetic fracture zone on the southeast side of the cave to study the effects of the interaction between two fractured zones around the cave on stress distribution and displacement.

Generally, fractures or joints decrease rock mass quality. In this numerical model, the fracture zone is modeled as rock mass with reduced strength and mechanical properties. The modulus of the fracture zone was modified to be 0.5 of that of the competent rock. In addition to property modification, determining the location of the fracture zone is crucial. This

information, predicted by the velocity distribution and changes in the cave boundary, requires regular updates through microseismic monitoring.

We oriented the planes by defining their dip and dip directions according to the relative strike of the lithologies, estimated at approximately N 40° E / 90° for both limestone-skarn and skarn-diorite boundaries. Additional planes were constructed to delineate the loosening and undamaged zones. As a result, the initial geometry was divided into multiple geometrical volumes. Specific properties, corresponding to their lithology and the conditions evident in the rock velocity model, were assigned to all segments of these geometrical volumes. This definition of lithology boundaries and rock mass conditions is a key step that supports the objectives of this modeling.

3. Results and discussion

The stress and displacement distribution at the cave boundary and surrounding rock mass have been modeled across three scenarios. The stress–strain results of scenario I elucidate the rock mass rheology. Subsequently, a comparison of displacement between scenarios I and II is discussed, focusing on the incorporation of the fractured zone and referencing measured TDR data on-site. Finally, the displacement results from scenario III are presented to describe rock mass behavior in response to interactions between the cave and the fracture zone.

3.1. Stress-strain distribution

The in situ stress applied in the model represents the gravitationally induced vertical stress, which is the major principal stress. This stress increases with depth. Block caving influences the stress condition of the underground rock mass. As shown in the vertical section of stress distribution in Figure 9, the in situ stress has been redistributed. Vertical section of stress distribution looking to the northeast (NW-SE section). The dotted white circles and line at the bottom of the cave indicate a high-pressure area where induced stress concentrates at the abutment of the undercut level. At the edge of the cave's top in the northwest (indicated by the red dotted circle), a compressional stress regime appears owing to the hanging rock. The dotted yellow circles indicate the area at the top of the cave where the stress regime operates under tension. Looking to the northeast, the section traverses the skarn lithology from northwest to southeast. The rock mass above the cave experiences tensile stress as a result of cave excavation. The area subjected to this tensile regime extends to a height approximately four times that of the cave. Above this tensile zone, a compression zone forms up to the upper boundary of the model, exhibiting a concave stress distribution. The compression regime that deepens with increasing depth appears to form along the sides of the cave.

The asymmetrical and irregular shape of the cave significantly influences the redistribution of induced stress. Besides the undercut level, which naturally bears the greatest compression load due to its position at the lowest cave elevation, compressive stress is also concentrated in the cave's contours. These high-stress compression concentration zones are characterized by tightly packed contour lines, observable on the northwest and southeast sides of the undercut level and in the middle side of the cave's northwest. The most significant compressive stress occurs at the corners of the undercut level tunnel, spreading laterally at the lowest elevation of the cave.

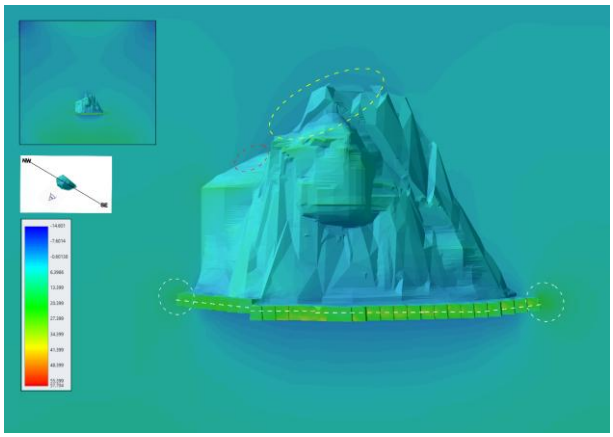

Figure 9. Vertical section of stress distribution

The redistribution of stress significantly impacts the rock mass strain. Above the cave, where the tensile stress regime is predominant, the modeled rock mass undergoes tensile strain towards the northwest and southeast. Correspondingly, in zones where compressive stress is concentrated, such as at the undercut level and along the cave ridge on the northwest side, compressive strain forms. The volumetric strain ranges from -0.0003 to 0.0014, reflecting the response of the hard rock mass to the distribution of induced stress. Vertical section of strain distribution, as shown in Figure 10, looking to the northeast (NW-SE section). The distribution of volumetric strain shows tensional strain at the top of the cave declining towards the northwest, following the cave shape. The area is bounded by a yellow dotted circle. Compression strain occurred at the undercut level (marked by the dotted white circle and lines) and at the edge of the top cave on the northwest, as indicated by the red dotted circle. The strain distribution corresponds to the stress distribution and is largely influenced by the irregular shape of the cave, particularly on the northwest side, where the cave's curvature deviates from that of the cave's top.

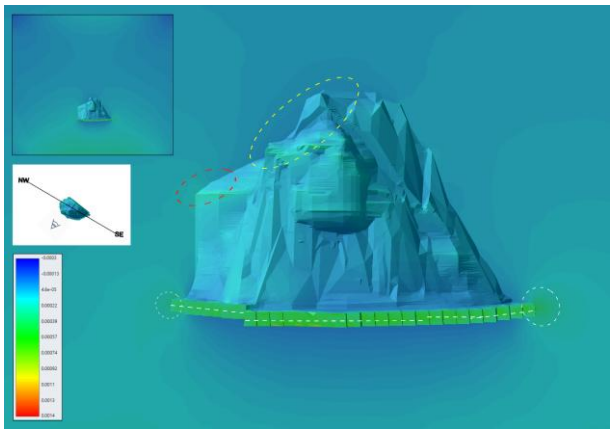

Figure 10. Vertical section of strain distribution

Displacement, a measurable response of rocks on-site, is compared with stress-strain analysis to validate rock mass behavior. Utilizing the evolution of cave shape recorded by the TDR measurements of Hidayat et al., 2024 [12] (Fig. 11), the model is validated. The displacement in numerical modeling indicates the distribution of cave expansion. Visualization of the DMLZ cave propagation section based on 57 d of TDR data. The brown, blue, yellow, and green lines represent the outer limits of the cave, updated bi-weekly.

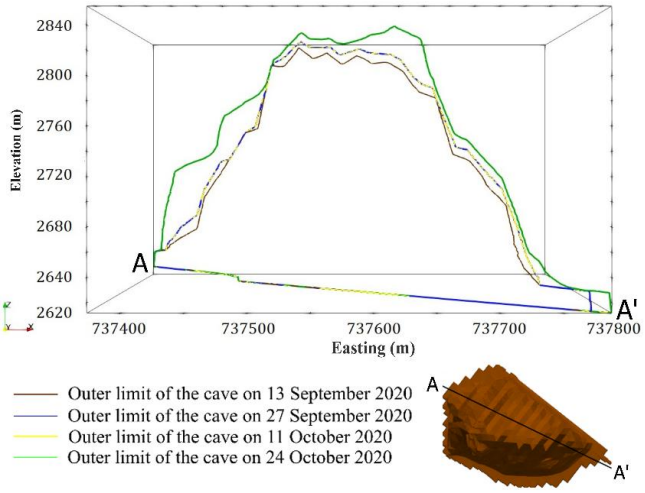

Figure 11. Visualization of the DMLZ cave propagation section based on 57 d of TDR data

The area between the brown and green lines indicates cave propagation over four weeks. The vertical cross-section looks to the northeast [12]. It indicates significant cave expansion in the northwest direction. Before cave pro-pagation occurs, displacement triggers movement until the collapse of the rock fraction from the insitu rock, with the predominant displacement distribution in the northwest direction where cave propagation is measured.

Figure 12 shows the displacement modeling for scenario I. The area bounded by the dotted white circles indicates the domi-nant displacement around the cave boundary. In scenario I, the largest displacement is at the top. Figure 13 shows the displacement modeling for scenario II. The area bounded by the dotted white circles indicates the dominant displacement around the cave boundary. Scenario II produces a concentration of displacement shifted marginally next to the northwest. The models tested, scenarios I and II, either without or with a loosening zone on the northwest side of the cave, respectively, demonstrate similar displacement distributions. The largest displacements, measuring 25 cm in scenario I and 26 cm in scenario II, formed over an area approximately five times the height of the cave (Figs. 12 and 13). This area marks the transition of the stress regime from tensile to compressive (Fig. 9).

From this center of maximum displacement to the top of the cave, displacement gradually decreases to as close as 18 cm in scenario I and 19 cm in scenario II.

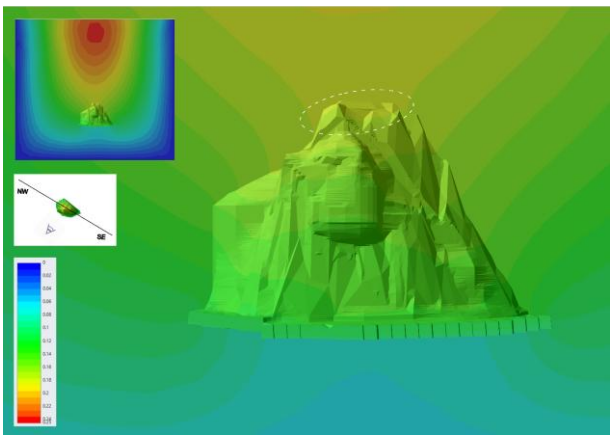

Figure 12. Displacement modeling for scenario I

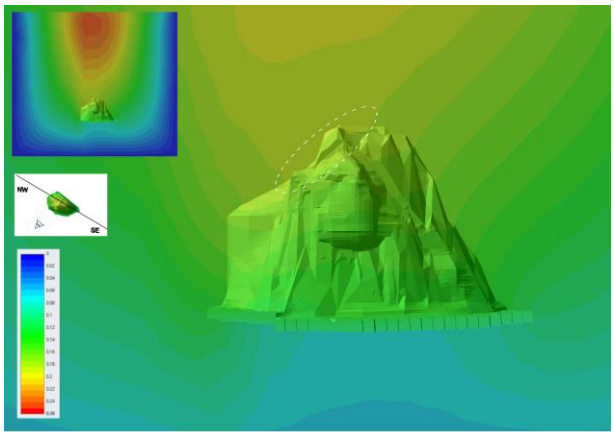

Figure 13. Displacement modeling for scenario II

Notable differences are observed in the area next to the northwest side of the cave. scenario II results in greater displacement on the northwest than scenario I, suggesting that in scenario II, the rock mass above the cave fails along the boundary of the cave on the northwest. Gravitationally, the shape of the rock that overhangs the side of the northwest cave experiences additional compression, acting as a new abutment above the undercut level. Corroborated by the cave propagation distribution in Figures 11 and 13, scenario II provides a displacement model that is more appropriately distributional than scenario I. This comparison demonstrates that the fracture zone, functioning as a loosening zone on the northwest of the cave in both models, contributes significantly to displacement around the cave. The fracture zone redistributes stress such that displacement is influenced not only by the cave shape and overburden pressure but also by the presence of the fracture zone within the rock mass.

Notably, the validation model used in this study was limited to the distribution of stress and displacement in terms of zonation, not their magnitude. Validation was achieved by correlating the area of dominant displacement with the area of cave propagation. Monitoring of cave geometry using TDR indicated cave propagation at the northwest boundary of the cave. Scenario II reflected this with dominant displacement in a zone similar to the area of cave propagation as indicated by TDR monitoring. This correspondence between the location of dominant cave propagation and displacement suggests that incorporating the fracture zone into the stress-displacement model could enhance predictions of cave propagation.

Compared to other numerical modeling methods for analyzing fracture or yielded zones around caves, such as adding stress to model elements [34] and experimenting with span variations adjusted to the caving mechanism [35], the approach proposed in this study aligns more closely with field conditions. This is because the location and properties of the fracture zone are estimated from the velocity model derived from monitoring results at the site. The integration of fracture zones based on velocity model information has facilitated a displacement distribution model informed by actual cave changes.

In the stress-strain-displacement analysis of hard rocks using the block caving method, modifying the rock mass property to be weaker in the loosening zone is strongly recommended. This modification enhances the accuracy of predictions regarding cave propagation locations. Once the treatment in this numerical model is considered sufficiently relevant and yields results validated by field measurements,

more complex simulations involving the presence of fracture zones can be undertaken.

Furthermore, our model considers the relative displacement due to material heterogeneities. For more precise results regarding the magnitude of stress and displacement, further studies involving calibration with rock mass data from the site and laboratory tests on rock samples are recommended.

3.2. Interaction of fracture zone and caves in hard rock mass

In block caving, rock engineering through preconditioning the hard rock mass is a key method for optimizing cave propagation performance. Selectively fracturing areas aids in controlling cave development to conform with the required mine design. In scenario III, the synthetic fracture zone represents both in situ fracture zones, such as faults or inherently weak rock masses, and constructed fracture zones, such as those created through hydrofracturing or destress blasting.

In this model, the synthetic fracture zone engineered on the southeast side of the cave acts in opposition to the loosening zone. Figure 14 shows the vertical section looking northeast in modeling scenario III. The loosening and synthetic fracture zones result in displacement that is evenly distributed on both the northwest and southeast sides of the cave. This arrangement causes displacement to extend beyond the cave, predominantly in the main southeast-northwest direction. This is evidenced by the range of displacement contour curves on the cave roof, which appear flatter and more expansive than those in scenarios I and II. On both the northwest and southeast sides, the displacement contours are uniformly distributed, providing an even balance of cave propagation in both directions.

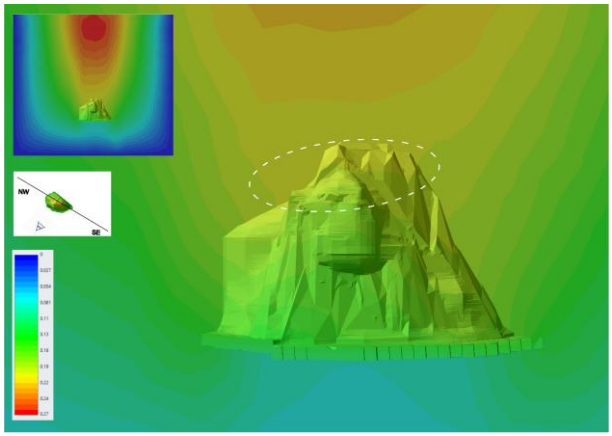

Figure 14. Vertical section looking northeast in modeling scenario III

The model configuration presented here successfully enhances the understanding that the fracture zone significantly influences the dominant displacement position, which in turn triggers cave propagation. If a fracture zone is positioned opposite the loosening zone, it can assist in balancing the location of cave propagation toward the top of the cave. In modern block caving engineering, where preconditioning can weaken the rock mass, the locations of preconditioning are crucial in determining the direction of cave propagation. For instance, if there is an existing weak rock mass around the cave, such as in the northwest zone (loosening zone), then a fracture zone in the southeast can be engineered through preconditioning to control the direction of propagation, ensuring it is more evenly distributed.

The model demonstrates that synthetic fracturing displaces the southeast or roof of the cave. According to the results, artificial fracture zones created by methods such as hydraulic fracturing can direct the displacement of rock mass, potentially triggering cave propagation at the cave roof and boundary. In the concept of cave mining, rock engineering is designed to achieve continuous caving in the direction specified by mine design. For vertically dipping deposits such as the DMLZ skarn system in this case study, controlling propagation to continue toward the cave roof in the direction of the deposit dip is crucial for sustaining efficient production and avoiding dilution. The synthetic fracture zone is highly recommended to be added along the strike of deposits and in the next block of the mining phase. If the propagation in the cave roof becomes stalled because the actual redistribution of caving-induced stress is insufficient to collapse the rock mass, synthetic fracturing can be implemented in a specific direction following mine planning. The extension of the cave area can increase stress and distribute displacement to trigger damage and fractures.

The model configuration described in Table 2 elucidates the influence of the fracture zone on the dominant displacement position that triggers cave propagation.

The modeling methods discussed can be applied to other sites to place fracture zones according to field conditions. The key to a representative model lies in positioning zones of loosening and fracture based on investigation and monitoring of the site's geotechnical characteristics. Comprehensive geotechnical investigations must precede the design of mine models to accurately represent the quality of rock masses and fault zones. Likewise, monitoring changes in the condition of rock masses due to induced block caving must be conducted continuously. This understanding of the interaction between the loosening and fracture zones will be useful for rock engineering in controlling the direction of cave propagation and engineering the fracture zone.

4. Conclusions

The integration of seismic velocity data into numerical modeling for cave propagation analysis has shown significant promise, as demonstrated by the 4D tomography approach. The strain analysis revealed tensile strain values reaching up to -0.0003 in the rock mass above the cave and compressive strain down to -0.0014 at the undercut level, demonstrating a realistic pattern of stress redistribution. This study found that incorporating a loosening zone in the second scenario improved the predictive accuracy of displacement modeling, aligning with observed TDR data. Specifically, the second scenario indicated a maximum vertical displacement of 19 cm near the northwest boundary of the cave, closely matching the TDR-measured cave propagation. In contrast, the first scenario, which did not include the weak zone, exhibited a less displacement (18 cm) and a less precise displacement distribution. These adjustments enhanced the model's capability to accurately reflect stress and displacement dynamics, increasing the reliability of predictions concerning actual cave behavior.

In the third scenario, the addition of a synthetic fracture zone on the southeast side balanced the displacement distribution across the cave, with a maximum observed displacement of 20 cm along the cave roof and a more uniform strain distribution.

Table 2. Summary and comparison of three modeling scenarios

Model's settings and result	Scenario I	Scenario II	Scenario III
Feature	Conventional modeling of cave	Advanced modeling incorporating fracture zones and cave	Engineering modeling analyzing the interaction of fracture zones and cave
Materials	Heterogenous: diorite, skarn, and limestone	Heterogenous: diorite, skarn, and limestone	Heterogenous: diorite, skarn, and limestone
Modified geometry	Lithology boundaries	Lithology boundaries, loosening zone	Lithology boundaries, loosening zone, and synthetic fracture zone
Modified properties	Lithology interface	Lithology interfaces and fracture zones	Lithology interfaces and fracture zones
Fractured zones	No fracture zone	Loosening zone in the northwest of cave	Loosening zone in the northwest and synthetic fracture zone in the southwest of cave
Dominant displacement	Top of cave's roof	Marginally shifted next to the northwest of cave's roof, confirmed by actual cave propagation from TDR data	Distributed to the northwest and southeast of cave's roof

This resulted in more controlled cave growth and demonstrated that strategic placement of fracture zones, could effectively guide cave propagation. By utilizing velocity tomography data, this study presents a refined numerical modeling approach for understanding rock mass behavior, contributing to safer and more efficient deep block caving operations. Future work should focus on calibrating these models with additional site-specific rock mass data and continuous monitoring to further enhance predictive accuracy and operational reliability.

Author contributions

Conceptualization: SM, RKW, DPS, GMS; Data curation: SM, WH, ER; Formal analysis: SM, RKW, DPS, GMS; Funding acquisition: SM, RKW, DPS, GMS; Investigation: SM, WH, ER; Methodology: SM, RKW, DPS, GMS; Project administration: DPS, ER; Resources: DPS, GMS, ER; Software: SM, AW, WH; Supervision: RKW, DPS, GMS; Validation: SM, RKW, DPS, GMS, WH, ER; Visualization: SM, WH; Writing – original draft: SM, DPS, GMS; Writing – review & editing: SM, RKW, DPS, GMS, AW. All authors have read and agreed to the published version of the manuscript.

Funding

This study work was funded in part by the Centre for Education Services (Pusat Layanan Pendidikan) under the Ministry of Education and Culture and the Indonesia Endowment Funds for Education (LPDP) awarded to Sari Melati [Grant number 202101122085]; Riset Unggulan ITB, awarded to Ridho K. Wattimena; Program Penguatan Inovasi ITB, awarded to David P. Sahara; and Revitalisasi Peralatan Laboratorium ITB, awarded to Ganda M. Simangunsong.

Acknowledgements

We would like to express our gratitude to the researchers in our groups: Geomechanics – Mining Engineering and Global Geophysics. Their invaluable knowledge and competence assisted us in dealing with this new issue. We also appreciate the staff and technicians at the Geomechanics and Mining Equipment Laboratory, Vulcanology and Geothermal Laboratory, Geophysical Instrumentation, and Electronics Laboratory for their assistance in providing us with the resources needed to conduct the research.

Conflicts of interest

The authors declare no conflict of interest.

Data availability statement

The original contributions presented in the study are included in the article, further inquiries can be directed to the corresponding author.

References

[1] Castro, R., Gómez, R., Hekmat, A. (2016). Experimental quantification of hang-up for block caving applications. *International Journal of Rock Mechanics and Mining Sciences*, *85*, 1-9. https://doi.org/10.1016/j.ijrmms.2016.02.005

[2] Espinoza, J.P., Mascaró, M., Morales, N., & Ruiz Del Solar, J. (2022). Improving productivity in block/panel caving through dynamic confinement of semi-autonomous load-haul-dump machines. *International Journal of Mining, Reclamation and Environment*, *6*(8), 552-573. https://doi/abs/10.1080/17480930.2022.2077046

[3] Catalan, A., Onederra, I., & Chitombo, G. (2017a). Evaluation of intensive preconditioning in block and panel caving – Part I, quantifying the effect on intact rock. *Mining Technology*, *126*(4), 221-239. https://doi.org/10.1080/14749009.2017.1300724

[4] Catalan. A., Onederra, I., Chitombo, G. (2017b). Evaluation of intensive preconditioning in block and panel caving – Part II, quantifying the effect on seismicity and draw rates. *Mining Technology*, *126*(4), 1-19. https://doi.org/10.1080/14749009.2017.1319527

[5] Li, G., Klein, B., Sun, C., & Kou, J. (2021). Insight in ore grade heterogeneity and potential of bulk ore sorting application for block cave mining. *Minerals Engineering*, *170*, 106999. https://doi.org/10.1016/j.mineng.2021.106999

[6] Noriega, R., Pourrahimian, Y., & Ben-Awuah, E. (2022). Optimization of life-of-mine production scheduling for block-caving mines under mineral resource and material mixing uncertainty. *International Journal of Mining, Reclamation and Environment*, *36*(2), 104-124. https://doi.org/10.1080/17480930.2021.1976010

[7] Flores, G., & Catalan, A. (2019). A transition from a large open pit into a novel "macroblock variant" block caving geometry at Chuquicamata mine, Codelco Chile. *Journal of Rock Mechanics and Geotechnical Engineering*, *11*(3), 549-561. https://doi.org/10.1016/j.jrmge.2018.08.010

[8] Eremenko, A.A., Mulev, S.N., & Shtirts, V.A. (2022). Microseismic monitoring of geodynamic phenomena in rockburst-hazardous mining conditions. *Journal of Mining Science*, *58*(1), 10-19. https://doi.org/10.1134/S1062739122010021

[9] Angin, P.P., Wattimena, R.K., Sahara, D.P., & Purba, A.M. (2019). Microseismic analysis to identify stress redistribution and minimize rockburst in DMLZ cave abutment, PT Freeport Indonesia. Proceedings of the *5th ISRM Young Scholars' Symposium on Rock Mechanics and International Symposium on Rock Engineering for Innovative Future*.

[10] Zhu, Q., Zhao, X., & Westman, E. (2021). Review of the evolution of mining-induced stress and the failure characteristics of surrounding rock based on microseismic tomography. *Shock and Vibration*, *1*, 2154857. https://doi.org/10.1155/2021/2154857

[11] Mercier, J.P., de Beer, W., Mercier, J.P., & Morris, S. (2015). Evolution of a block cave from time-lapse passive source body-wave traveltime tomography. *Geophysics*, *80*(2), 85-97. https://doi.org/10.1190/geo2014-0155.1
[12] Hidayat, W., Sahara, D.P., Widiyantoro, S., Suharsono, S., Riyanto, E., Nukman, M., Wattimena, R.K., Melati, S., Sitorus, E., Nainggolan, T., & Putra, I.P.R.A. (2024). 4D time lapse tomography for monitoring cave propagation and stress distribution in Deep Mill Level Zone (DMLZ) PT Freeport Indonesia. *Geomechanics and Geophysics for Geo-Energy and Geo-Resources*, *10*, 39. https://doi.org/10.1007/s40948-023-00718-w
[13] Garia, S., Pal, A.K., Nair, A.M., & Ravi, K. (2020). Elastic wave velocities as indicators of lithology-based geomechanical behaviour of sedimentary rocks: an overview. *SN Applied Sciences*, *2*, 1-21. https://doi.org/10.1007/s42452-020-03300-1
[14] Hua, D., Jiang, Q., Liu, R., Gao, Y., & Yu, M. (2021). Rock mass deformation modulus estimation models based on in situ tests. *Rock Mechanics and Rock Engineering*, *54*, 5683-5702. https://doi.org/10.1007/s00603-021-02578-w
[15] Lozovyi, S., & Bauer, A. (2019). Velocity dispersion in rocks: A laboratory technique for direct measurement of P-wave modulus at seismic frequencies. *Review of Scientific Instruments*, *90*(2), 024501. https://doi.org/10.1063/1.5026969
[16] Yasar, E., & Erdogan, Y. (2024). Correlating sound velocity with the density, compressive strength and Young's modulus of carbonate rocks. *International Journal of Rock Mechanics and Mining Sciences*, *41*(5), 871-875. https://doi.org/10.1016/j.ijrmms.2004.01.012
[17] Cai, M., Kaiser, P.K., Uno, H., Tasaka, Y., & Minami, M. (2004). Estimation of rock mass deformation modulus and strength of jointed hard rock masses using the GSI system. *International Journal of Rock Mechanics and Mining Sciences*, *41*(1), 3-19. https://doi.org/10.1016/S1365-1609(03)00025-X
[18] Karaman, K., Cihangir, F., & Kesimal, A. (2015). A comparative assessment of rock mass deformation modulus. *International Journal of Mining Science and Technology*, *25*(5), 735-740. https://doi.org/10.1016/j.ijmst.2015.07.006
[19] Khabbazi, A., Ghafoori, M., Lashkaripour, G.R., & Cheshomi, A. (2023). Estimation of the rock mass deformation modulus using a rock classification system. *Geomechanics and Geoengineering*, *8*(1), 46-52. https://doi.org/10.1080/17486025.2012.695089
[20] Deere, D.U., & Deere, D.W. (1989). *Rock quality designation (RQD) after twenty years*. US Army Engineer Waterways Experiment Station.
[21] Zhang, L. (2017). Evaluation of rock mass deformability using empirical methods – A review. *Underground Space*, *2*(1), 1-15. https://doi.org/10.1016/j.undsp.2017.03.003
[22] Duplancic, P., & Brady, B.H. (1999). *Characterisation of caving mechanisms by analysis of seismicity and rock stress*. ISRM Congress.
[23] Singh, M., Rao, K.S., & Ramamurthy, T. (2002). Strength and deformational behaviour of a jointed rock mass. *Rock Mechanics and Rock Engineering*, *35*(1), 45-64. https://doi.org/10.1007/s006030200008
[24] Zhang, L. (2010). Estimating the strength of jointed rock masses. *Rock Mechanics and Rock Engineering*, *43*, 391-402. https://doi.org/10.1007/s00603-009-0065-x
[25] Cumming-Potvin, D., Wesseloo, J., Jacobsz, S.W., & Kearsley, E. (2016). Fracture banding in caving mines. *Journal of the Southern African Institute of Mining and Metallurgy*, *116*(8), 753-761. https://doi.org/10.17159/2411-9717/2016/v116n8a7
[26] Rafiee, R., Ataei, M., Khalookakaie, R., Jalali, S.E., Sereshki, F., & Noroozi, M. (2018). Numerical modeling of influence parameters in cavability of rock mass in block caving mines. *International Journal of Rock Mechanics and Mining Sciences*, *105*, 22-27. https://doi.org/10.1016/j.ijrmms.2018.03.001
[27] Alipenhani, B., Majdi, A., & Bakhshandeh Amnieh, H. (2022). Determination of caving hydraulic radius of rock mass in block caving method using numerical modeling and multivariate regression. *Journal of Mining and Environment*, *13*(1), 217-233. https://doi.org/10.22044/jme.2022.11589.2149
[28] Castro, R.L., Gonzalez, F., & Arancibia, E. (2009). Development of a gravity flow numerical model for the evaluation of drawpoint spacing for block/panel caving. *Journal of the Southern African Institute of Mining and Metallurgy*, *109*(7), 393-400. https://doi.org/jsaimm/v109n7/01
[29] Li, L.C., Tang, C.A., Zhao, X.D., & Cai, M. (2014). Block caving-induced strata movement and associated surface subsidence: A numerical study based on a demonstration model. *Bulletin of Engineering Geology and the Environment*, *73*, 1165-1182. https://doi.org/10.1007/s10064-014-0656-y
[30] Cumming-Potvin, D., Wesseloo, J., Jacobs, S.W., & Kearsley, E. (2018). A re-evaluation of the conceptual model of caving mechanics. *Caving 2018: Proceedings of the 4th International Symposium on Block and Sublevel Caving, Australian Centre for Geomechanics*, 179-190. https://doi.org/10.36487/ACG_rep/1815_11_Cumming-Potvin
[31] Widodo, S., Anwar, H., & Syafitri, N.A. (2019). Comparative analysis of ANFO and emulsion application on overbreak and underbreak at blasting development activity in underground Deep Mill Level Zone (DMLZ) PT Freeport Indonesia. *IOP Conference Series: Earth and Environmental Science*, *279*(1), 012001. https://doi.org/10.1088/1755-1315/279/1/012001
[32] De Beer, W., Jalbout, A., Riyanto, E., Ginting, R., Sullivan, M., & Collins, D.S. (2017). The design, optimisation, and use of the seismic system at the deep and high-stress block cave Deep Mill Level Zone mine. *UMT 2017: Proceedings of the 1th International Conference on Underground Mining Technology, Australian Centre for Geomechanics*, 233-245. https://doi.org/10.36487/ACG_rep/1710_18_Collins
[33] Primadiansyah, A., Soumilena, N., & Teweng, W. (2020). Driving and managing stress in the Deep Mill Level Zone caving mine. *Proceedings of the Eighth International Conference & Exhibition on Mass Mining*, 394-405. https://doi.org/10.36487/ACG_repo/2063_25
[34] Board, M., & Pierce, M.E. (2009). A review of recent experience in modeling of caving. *Proceedings of the international workshop on numerical modeling for underground mine excavation design*, *9512*, 19-28.
[35] Alipenhani, B., Bakhshandeh Amnieh, H., & Majdi, A. (2023). Application of finite element method for simulation of rock mass caving processes in block caving method. *International Journal of Engineering*, *36*(1), 139-151. https://doi.org/10.5829/IJE.2023.36.01a.16

Моделювання розвитку зони обвалення при глибинній системі блокового обрушення з урахуванням зони тріщиноутворення, визначеної за даними сейсмічної томографії

С. Мелаті, Р.К. Ваттімена, Д.П. Сахара, Г.М. Сімангунсонг, А. Вібово, В. Хідаят, Е. Ріянто

Мета. Дослідження спрямоване на вдосконалення контролю за розвитком процесу обвалення при веденні гірничих робіт системою блокового обвалення порід шляхом інтеграції мікросейсмічної томографії у чисельне моделювання еволюції напружено-деформованого стану масиву порід та розподілу зміщень.

Методика. Використано низькошвидкісну зону, виявлену за допомогою чотиривимірної томографії, як область тріщиноутворення або розущільнення поблизу межі обвалення. Для аналізу впливу на розподіл напружень та зміщень були скориговані пружні властивості цієї зони. Моделі зміщень для кожного сценарію були верифіковані за даними відбивальної рефлектометрії у часовій області (TDR).

Результати. Виявлено, що зниження модуля деформації масиву порід, визначене за зменшенням швидкості сейсмічних хвиль, забезпечило відповідність розподілу зміщень результатам вимірювань TDR. Встановлено, що кількісне зменшення модуля деформації у зоні розущільнення з низькою швидкістю (4.5 км/с) становить приблизно 0.5 від модуля суцільних порід. Північно-західна межа обвалення, прогнозована як зона найбільшого зміщення (19 см), була точно змодельована, що узгоджується з підвищеною концентрацією напружень та локалізацією напружено-деформованого стану в цій області.

Наукова новизна. У роботі запропоновано новий інтегрований підхід, який використовує швидкісні моделі масиву, отримані з мікросейсмічного моніторингу, для коригування модуля деформації в чисельному моделюванні на етапі тріщиноутворення під дією високих напружень, зумовлених обваленням. Відмінність підходу полягає у тому, що традиційні чисельні моделі "напруження – деформації – зміщення", зазвичай, враховують сталі властивості масиву порід, Проте, у процесі обвалення інтенсивне розростання та поширення тріщин перетворюють масив із монолітного на сильнотріщинуватий, що суттєво змінює його механічну поведінку.

Практична значимість. Оптимізовано використання даних мікросейсмічного моніторингу для актуалізації стану масиву порід у зоні тріщиноутворення. Запропонований підхід дозволяє зробити пружні властивості у чисельному моделюванні більш репрезентативними у часі та врахувати вплив розвитку тріщинуватості.

Ключові слова: *розвиток обвалення, зони тріщиноутворення, чисельне моделювання, сейсмічна томографія, підземна розробка родовищ*

Publisher's note

All claims expressed in this manuscript are solely those of the authors and do not necessarily represent those of their affiliated organizations, or those of the publisher, the editors and the reviewers.